Journal of the European Ceramic Society **18** (1998) 857–870

PII: S0955-2219(97)00210-0
0955-2219/98/$19.00 + 0.00

The Thermal Gradient—Pulse Flow CVI Process: a New Chemical Vapor Infiltration Technique for the Densification of Fibre Preforms

S. Bertrand,* J. F. Lavaud, R. El Hadi, G. Vignoles and R. Pailler

Laboratoire des Composites Thermostructuraux (UMR 47 CNRS-SEP-UB1), Domaine Universitaire, 3 Allée de la Boëtie, 33600 Pessac, France

(Received 12 September 1997; accepted 20 November 1997)

Abstract

Three-dimensional carbon fibre preforms were infiltrated with pyrocarbon or silicon carbide using a new process which combines a thermal gradient variation with a pressure pulsed chemical vapor infiltration. In this work, the principle of this TP–CVI process is presented. Thermal evaluations are carried out as guidelines to set up a model. Experimental infiltrations were performed, to validate the model. A comparison with experiments performed by P–CVI (i.e. without thermal gradient) shows that the TP–CVI process yields a better in-depth densification of the preform and a better deposit homogeneity. The thickness gradient depends chiefly on the thermal quenching ΔT. *Process and equipment improvements led to samples more densified in the core than near the surface, that is, to samples still densifiable after considerable densification. This new technique also allows the use of preforms with higher fibre volume fractions.* © *1998 Elsevier Science Limited. All rights reserved*

1 Introduction

For 30 years, the Chemical Vapor Infiltration (CVI) process has been recognized as one of the most convenient methods for the fabrication of fibre-reinforced Ceramic Matrix Composites (CMCs) containing staple or continuous fibres. The interphase and/or the matrix of such materials, e.g. carbon or a refractory carbide, nitride or oxide, are deposited in the fibrous preform via a heterogeneous gas–solid reaction taking place on the wall of the heated preform pores. The steps of the CVI process are as follows: (1) the fibrous preform is placed in a high temperature furnace, (2) gaseous reactants (also referred to as precursors) are allowed to flow inside the deposition chamber, (3) they (or their decomposition products acting as intermediate species) diffuse inside the porous preform, (4) and react with each other on the hot substrate (the surface of the fibres), producing a solid deposit and gaseous by-products.

Different types of CVI processes have been described for the preparation of fibrous CMCs,[1,2] as summarized in Fig. 1.

The first process is the isothermal–isobaric CVI (denoted as I–CVI):[3,4] the preforms are maintained at a uniform temperature, and the reactants flow through the furnace and around the preform, penetrating inside it mainly by diffusive transport. One of the main drawbacks of this process is that matrix deposition occurs preferentially near the surface of the substrate, leaving the interior of the preform poorly densified. The resulting material does not display optimal mechanical properties. To alleviate this drawback, the gas pressure must be reduced in order to enhance the diffusive transport with respect to the chemical reaction rate. However, one has to face an optimization problem since the infiltration time is considerably increased under such low deposition rate conditions.

The second process, thermal gradient isobaric CVI (T–CVI), is aimed at avoiding the aforementioned problem by the use of a steep thermal gradient throughout the preform. As the chemical deposition reaction is strongly thermally activated, appreciable amounts of solid will only be deposited near the hot side of the preform, preserving an access to the pores by the cold side. However, as

*To whom correspondence should be addressed.

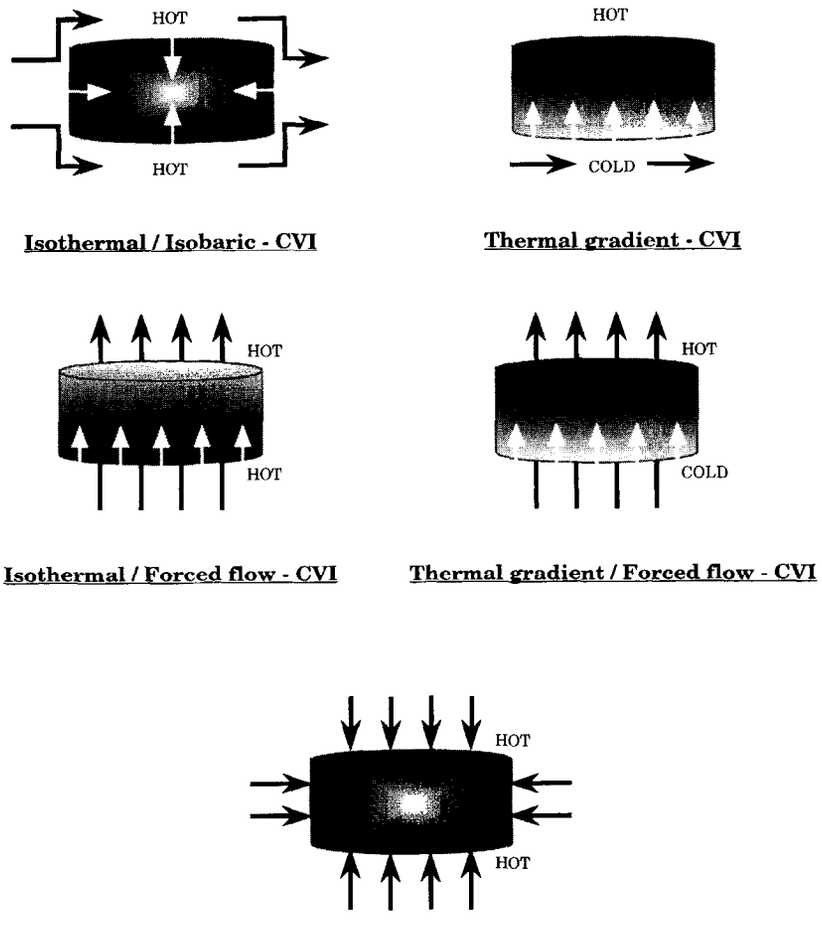

Fig. 1. Different types of CVI process. The black arrows represent flowing reagents, and the white arrows show reagent diffusion. The densification gradient is indicated by the shading. The heavier shading denotes more deposition.

the deposition front moves towards the cold side, the efficiency of the process decreases, but still leads to important overall densification times.

In the third process, isothermal forced-flow CVI (denoted F–CVI),[3–6] the reactants are forced to flow through an isothermally heated preform. This technique allows rapid deposition inside the whole preform, but since the precursor concentration decreases between the entrance and exit of the pores, it is not possible to avoid some densification gradient. Other drawbacks of this process are the necessity to treat only one preform at a time, the impossibility to handle complicated preform geometries, the persistence of a densification gradient at the end of the process, due to early pore plugging at the exit face, and a less efficient densification of fine pores with respect to larger ones, owing to the convective character of precursor transport.

Combining the T–CVI and the F–CVI leads to the fourth process, the thermal-gradient forced-flow CVI (denoted as TF–CVI).[7] Reactants enter the preform by its cold face, and flow towards regions of the substrate which are hot enough to promote chemical deposition. A better final homogeneity and an infiltration time reduction are the major advantages of this technique, due to a high renewal rate of the precursor gases within the pore network of the preform. Nevertheless, the drawbacks of T–CVI and F–CVI such as their lack of flexibility are not totally overcome.

Another direction of improvement is the pressure-pulsed CVI technique (P–CVI).[8–11] This process is based on the repetition of pressure cycles. Each cycle consists of: (1) gas evacuation from the reactor, (2) quasi-instantaneous introduction of the reactants, and (3) a hold-on period during which the gases diffuse inside the preform and react (Fig. 2). When the reaction rate decreases, owing to reactant depletion as well as gaseous by-products formation, a new cycle begins. Accordingly, the renewal of the precursor gas is achieved at a high rate, and the deposition rate increases, leading to somewhat shorter operation times.[12,13] However, a densification gradient still remains.

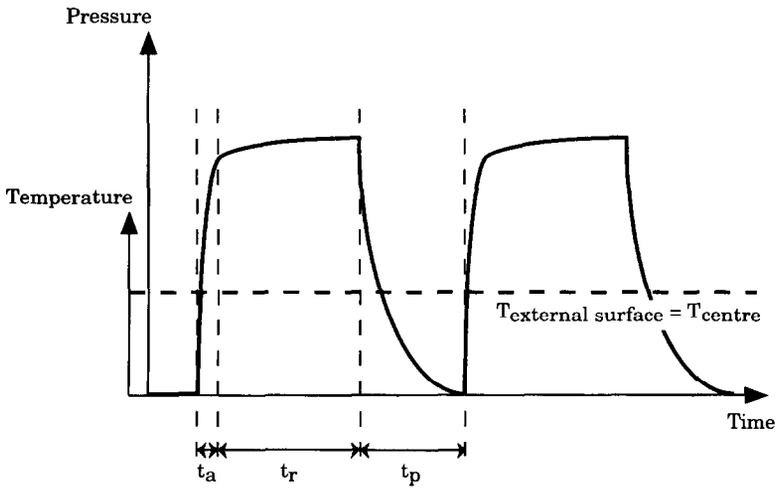

Fig. 2. Temperature and pressure variations with time in conventionnal P–CVI process. (t_a: reactants admission; t_r: residence time; t_p: evacuation step).

Summarizing the CVI techniques, it appears that the basic one, I–CVI, although it has an extremely high flexibility also displays several main drawbacks including: a densification gradient and a significant residual porosity in the resulting composite material, and relatively long infiltration times. The infiltration times decrease when using the other methods presented above, and particularly the F–CVI route. Using the appropriate method, fibrous preforms with many types of architectures, geometries, and fibre nature have been successfully infiltrated with carbon or ceramic matrices. However, in every case, the composites display some residual porosity (typically 10–15%) and a densification gradient from the inside to the outside (or from one side to the other), prejudicial to their mechanical properties.

In order to reduce or invert such a gradient, a new CVI process has been recently developed at LCTS. This technique consists in creating temporarily an inverted thermal gradient in the preform (i.e. a 'cold' surface and a 'hot' core) and to take advantage of this state to apply one or more pressure pulses.

This paper is devoted to the description of this new process. It is divided into two main parts: (1) a description of the basis of the process and computational evaluations, and (2) a description of the experimental setup, as well as a presentation and a discussion of the results.

2 Principle of TP–CVI

As already mentioned for T–CVI, the presence of a thermal gradient may be suitable to an enhancement of the deposition efficiency, as soon as the operating conditions lie in the chemical control region, i.e. the region of parameters space where the overall deposit rate is limited by the chemical reaction kinetics rather than by diffusive transport. Indeed, in this case, the temperature dependence is strong (through Arrhenius-like laws), so one expects the effect of a temperature gradient on the local deposition rate to be very strong. In particular, if it is possible to achieve a higher temperature in the less accessible regions of the porous network, the problem of early pore plugging may be drastically reduced. In T–CVI the choice has been made to keep one side of the preform hotter than the other, but this strategy relies on the assumption that the preform geometry is simple enough, and it leads to a strong dissymmetry between the two sides. Less harmful to the mechanical properties and insensitive to the preform geometry would be simply to remove the preform from the hot zone of the furnace, and let it exchange heat with its surroundings through its surface: indeed, a convenient thermal gradient appears during the whole cooling time. Accordingly, our choice has been to set the preforms on a piston which allows them to stay inside or apart from the furnace hot zone. A TP–CVI cycle may be then composed as follows (Fig. 3):

1. While the deposition chamber is held under vacuum, the preform lies in the hot zone, and its temperature becomes high and uniform.
2. The preform is moved away from the hot zone by the piston: a temperature gradient progressively appears as it cools down.
3. After some gradient setup time t_g, the gaseous reactants are introduced, during an admission time t_a, in a quasi-instant pressure pulse.
4. The reactive gases are kept inside the deposition chamber during a given residence time t_r, during which deposition occurs.
5. The gases are then removed by the outlet during an evacuation (or pumping) time t_p.

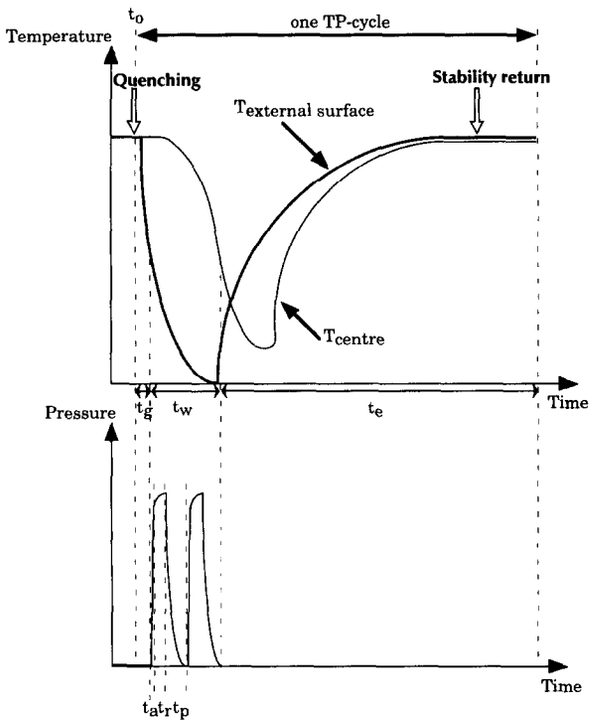

Fig. 3. Temperature and pressure variations with time in a TP–CVI process (example for a two-pulsed-mode). (t_a: reactants admission; t_r: residence time; t_p: evacuation step; t_w: total time of P–CVI cycles, during a temperature quenching interval; t_e: stability time; t_g: temperature gradient establishment).

6. The pulse–CVI cycle ($t_w = t_a + t_r + t_p$) is repeated if the temperature gradient still is steep enough.
7. Then the preform is reset with the piston in the hot zone to be heated again as in step (1).

3 Thermal Evaluations

3.1 Model setup

A first evaluation of the potentiality of the process was achieved through thermal computations, in order to quantify the 'useful' part of the preform cooling history, that is, the time period after the removal of the preform from the hot zone where the temperature gradient from the center to the surface is significant enough to lead to a more efficient densification. Accordingly, a simplified model has been set up with the following hypotheses:

1. H1—When the gas flows in the furnace, it displays low enough Reynolds number (typically less than 10) to assume a laminar, Poiseuille-like behaviour outside the preform.
2. H2—As the preform permeability is low, the gas velocity inside the preform is negligible, so the main mode of heat exchange between the gas and the preform surface is essentially conductive.
3. H3—It is assumed that the heat exchange between gas and solid at the porous medium interface is efficient enough to consider only one averaged temperature for the gas and the solid, the conductivity and heat capacity of this composite medium being simply approximated by a law of mixtures.

All these hypotheses joined together form the following heat equation:

$$\rho C_p \partial T/\partial t + \nabla.(\underline{\underline{k}}\nabla T) + \rho C_p \mathbf{v}.\nabla T = 0 \qquad (1)$$

The first term on the left-hand side is the accumulation term, the second describes heat conduction, the third heat convection due to gas flow, and the right-hand side is a volumic heat source term. ρ stands for the density, C_p for the mass heat capacity, $\underline{\underline{k}}$ the heat conductivity tensor, and $\mathbf{v}$ the gas velocity vector. Equation (1) is completed by the specification of convective and radiative boundary conditions for the preform and the deposition chamber wall:

$$(\underline{\underline{k}}\nabla T).\mathbf{n} = H(T_S - T\infty) + qr \qquad (2)$$

where H is a heat exchange parameter, T_S is the unknown temperature at the exchange surface, and $T\infty$ the temperature of the heating or cooling fluid. The radiative flux qr is obtained through the consideration of a radiating cavity model formed of NS surface elements:

$$qr = \sum_{i=1}^{NS}\sum_{j=1}^{NS} q_{ij} \qquad (3)$$

where the element-to-element contributions are expressed as:

$$q_{ij} = \left(\sigma e_i T_i^4/\pi\right) A_i \left(\cos\Phi_i \cos\Phi_j A_j / r_{ij}^2\right) = J_i A_i F_{ij} \qquad (4)$$

where A_i being the area of element i, J_i its emissive power, and F_{ij} the geometric viewfactor between elements i and j, computed using the angles to the normal vectors Φ_i and Φ_j and the mutual distance r_{ij}.

The geometry used for the numerical simulation is described in Fig. 4: it is a simplified view of a tubular reactor, with the preform inside it. We describe a totally axisymmetric problem to keep a reasonable computer time per run, also knowing that a very precise approach is still beyond our scope. In the case of no gas flow, an extra simplification has been brought by introducing a

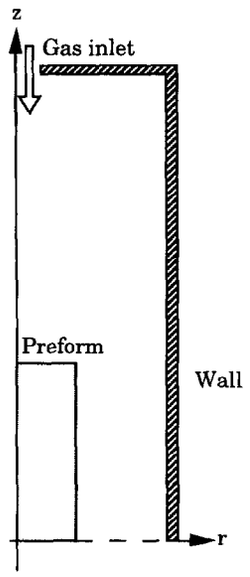

Fig. 4. Axisymmetric geometry used for the computational approach.

horizontal symmetry plane: accordingly, the thermal cycles are represented by alternatively setting the wall temperature at a high and an ambient value.

As we were not primarily interested in the mechanics and thermal behaviour of the gases, a simple approximate model has been used. The void space between the preform and the walls has been assimilated to a channel where a fluid circulates at a given velocity, with a given heat exchange parameter H. The solving of eqn (1) is not performed inside the fluid. On the other hand, concerning radiation computations, the gas has been assigned a low emissivity of 0·1 to simulate a screening effect.

The various properties of the preform were estimated from the known properties of the T300 fibres (from Torayca, Japan) which constitute it. All the numerical parameters of the simulation are grouped in Table 1. Many of the given values are only estimated at ambient temperature, and assumed not to vary with it. The thermal conductivity of the preform has been computed using the following formula:

$$K_{\text{eff}} = \frac{fK_{//}}{F} \qquad (5)$$

where f is the fibre volume fraction, $K_{//}$ the longitudinal conductivity of the fibres (6·5 W m^{-1} °C^{-1}), and F a formation factor. Values of F have been computed for isotropic 3-directional random arrays of freely overlapping conductive fibres.[14] For a fibre volume fraction of 0·3, the formation factor is 7·6.

3.2 Model validation

The above equations, geometry, and data set have been validated by comparing the evolution of the temperature in the center of the preform during heating and cooling phases with no gas flow (that is, with radiation being the only heat exchange mode between the preform and the walls), with experimental data. Figure 5 shows the comparison between computed and measured temperatures for heating and cooling runs with various imposed gradients. The simulations were carried out both with a constant temperature at the walls and with decreasing temperatures away from the preform, and the results remained essentially unaltered. Accordingly, a constant temperature schema has been retained for all computations presented here. The calculated time–temperature curves are in excellent agreement with the experimental data.

3.3 Effective thermal gradient evaluation

In addition to the time–temperature curves for the center of the preform, the computations also yield a time evolution for the complete temperature field in the preform. For example, Fig. 6 is a plot of the temperature profile along the radial direction (in the narrowest dimension of the preform) varying with time. This plot allows to visualize the progression of a cooling front towards the center of the preform.

A simple exploitation of these results has been carried out in terms of the temperature difference between the center and the external surface of the preform. Figure 7(a) shows the time evolution of this temperature difference for various imposed gradients. The necessary time for this difference to be appreciable is very short, i. e. a few seconds or less. The difference goes then to a maximum at $t\#6$ s, more or less at the same time when the cooling

Table 1. Data values for the heat transfer evaluations

Parameters	*Preform*	*Walls*	*Gas (propane)*
Preform dimensions	h = 32 mm Ø = 15 mm		
Volumic mass	0·5 10^3 kg m^{-3} (fiber volume fraction ≈0·3)	3·0 10^3 kg m^{-3}	
Specific heat capacity	7·1 10^2 J kg^{-1} °C^{-1}	7·1 10^2 J kg^{-1} °C^{-1}	
Thermal conductivity	≈ 0·25 W m^{-1} °C^{-1}	6·0 W m^{-1} °C^{-1}	
Emissivity	0·8	0·8	0·1
Convective heat transfer coefficient between gas and solids			5 10^{-5} J °C^{-1} s^{-1} m^{-2}

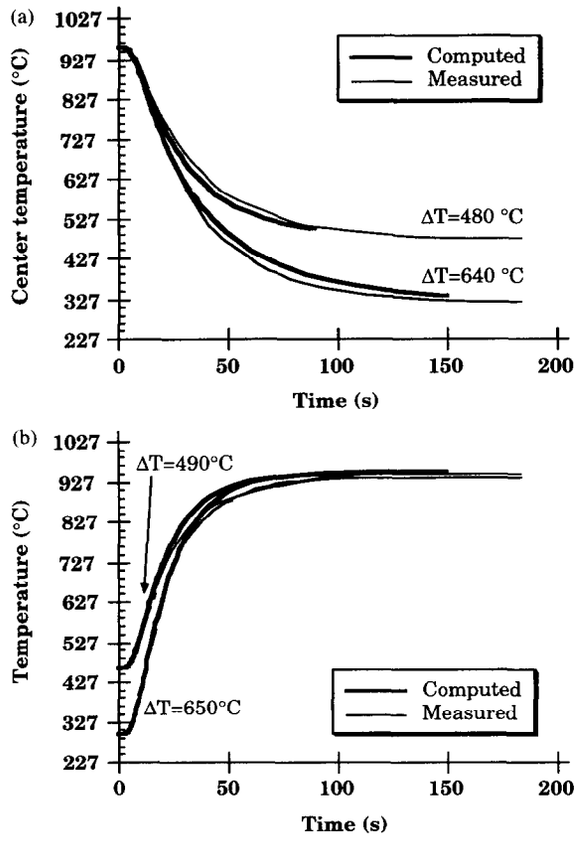

Fig. 5. Temperature at the center of the preform during cooling (a) and heating (b) experiments in an empty furnace. The preform was initially held at a uniform temperature and then was placed in a cooler or hotter ambient. (Computations were performed according to the text, with the geometry of Fig. 4 and the values of Table 1).

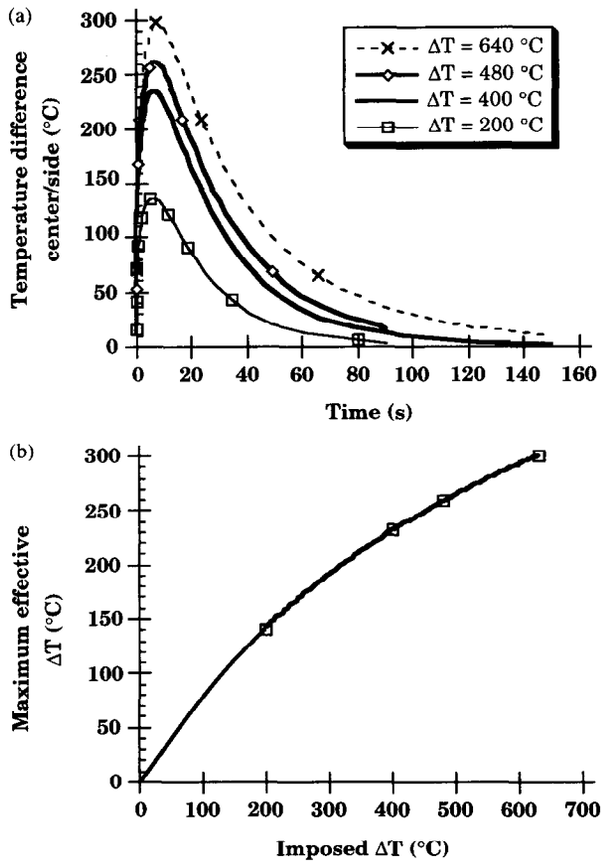

Fig. 7. Time evolution of the temperature difference between the center and the closest border of the preform, for various values of the applied gradient (a), and evolution of the maximal effective gradient as a function of the imposed temperature difference for cooling runs starting at $T = 950°C$ (b).

front reaches the center, followed by an exponential-like decay. The maximal effective ΔT has been plotted against the imposed ΔT in Fig. 7(b), giving some kind of maximal thermal efficiency curve.

3.4 Evaluation of the influence on chemical kinetics

Once the thermal behaviour of the preform is known, it may be translated into a chemical kinetic behaviour, with the help of some basic assumptions. As our goal is only to guess tendencies, we will try to interpret the thermal results by a direct use of the Arrhenius law. According to it, a temperature difference ΔT apart from T_0 will shift the value of a chemical rate factor k from k_0 in the following manner:

$$\ln\left(\frac{k_0}{k}\right) = \frac{E_a}{RT_0} \cdot \frac{\Delta T}{T_0 - \Delta T} \tag{6}$$

where E_a is the activation energy and R the perfect gas constant.

If ΔT represents the maximal effective center-to-surface thermal difference, then k_0/k is a center-to-surface rate efficiency factor, that will be renamed k_c/k_s. The question is: what minimal value this ratio should have in order to invert the densification gradient? Actually, one necessary condition for the inversion of the gradient is that the instant deposition rate ratio R_c/R_s is superior to 1. For a first-order reaction, it is equal to k_c/k_s multiplied by the center-to-surface active species concentration ratio c_c/c_s. Since c_c/c_s is usually much lower than 1, for example 10^{-1}, k_c/k_s has to exceed at least a value of 10 to lead to an actual inversion of the densification gradient. Other factors also enhance the critical value:

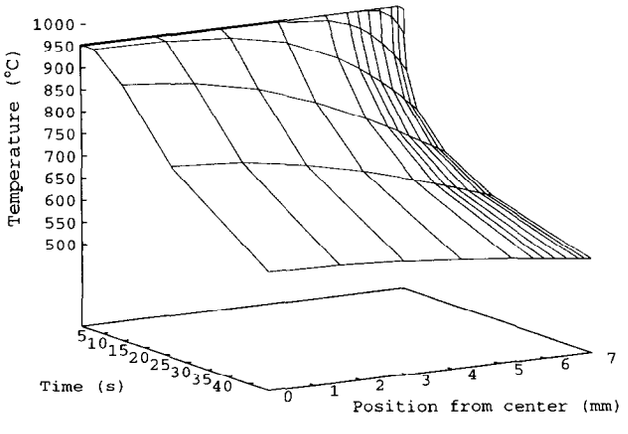

Fig. 6. 3D plot of temperatures versus radial position and time. The lines on the base plane are isothermal contours.

1. The ΔT accounted for in the computation is the maximal achievable ΔT, and not an averaged value on the 'useful' part of the pulse—since we need to know already the value of the criterion to assess which part of the pulse has to be used.
2. During inverse-gradient densification, the thermal diffusivity $k/\rho C_p$ of the preform increases with time, leading to lesser effective ΔT and faster cooling cycles. For instance, when the fibre volume fraction goes from 30 to 90%, the effective thermal conductivity varies by a factor of 17, while the product ρC_p varies only by a factor of 3. For an imposed ΔT of 200°C, we have estimated that the effective maximal ΔT goes from 136°C at $f=30\%$ to 60°C at $f=90\%$.

According to these considerations, we may increase the critical value of k_c/k_s up to 100. Figure 8 is a plot of $\log(k_c/k_s)$ as a simultaneous function of the imposed ΔT and the activation energy of the process. It can be seen readily that the activation energy of the densification reaction plays a major role for the definition of working conditions suitable to an inverted gradient densification. Indeed, we can guess from this graph that the TP–CVI of carbon is only feasible with severe gradients (>400°C), while more moderate values are satisfactory for SiC growth (at least in the low-temperature, high-E_a regime).[15]

Once a k_c/k_s criterion has been set, it is possible to estimate the time intervals during which the densification will be quicker in the center than near the surface, that is, (t_r+t_p) in Fig. 3. Equation (6) and the criterion $k_0/k=k_c/k_s\geq 100$, may be rewritten in the following way:

$$\frac{1}{RT_0}\cdot\frac{\Delta T}{T_0-\Delta T}\geq\frac{\ln(100)}{E_a} \tag{7}$$

Figure 9(a) is a plot of the left-hand side of eqn (7) against time. The horizontal lines are critical values corresponding to carbon deposition ($E_a\#200\,\text{kJ mol}^{-1}$) and SiC deposition ($E_a\#700\,\text{kJ mol}^{-1}$). The crossings of the curves with these lines yield the initial and final times for useful pulsing. Figure 9(b) shows the evolution of the useful time window for inverted gradient deposition, as a function of the imposed temperature difference.

3.5 Scaling considerations

One important point is the question of the capability of such process to be extended up to an industrial scale; that is, do larger reactor and preform size lead to equally or more efficient thermal gradients?

A short glance to the simplified heat conduction equation $\rho C_p \partial T/\partial t + \nabla.(\underline{\underline{k}}T) = 0$ brings one to the conclusion that if the dimensions are multiplied by a factor of 10, then the time required to reach a quasi-homogeneous temperature distribution in the

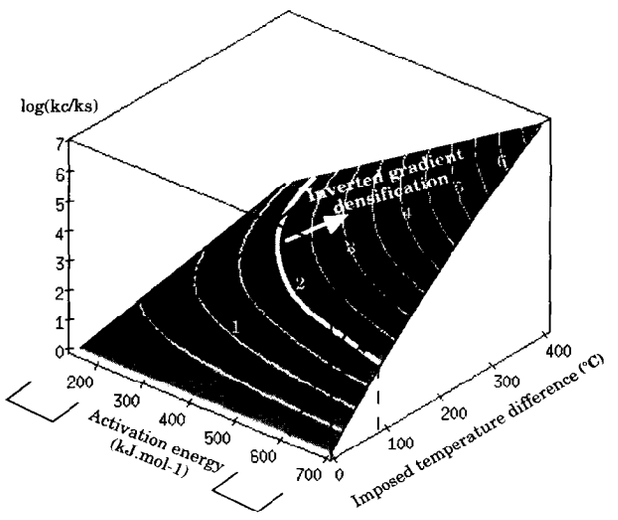

Fig. 8. Plot of the center-to-surface kinetic factor ratio versus activation energy and imposed temperature gradient at $T_c=950$°C. The $k_c/k_s=100$ level has been highlighted as a possible criterion for inverse gradient densification.

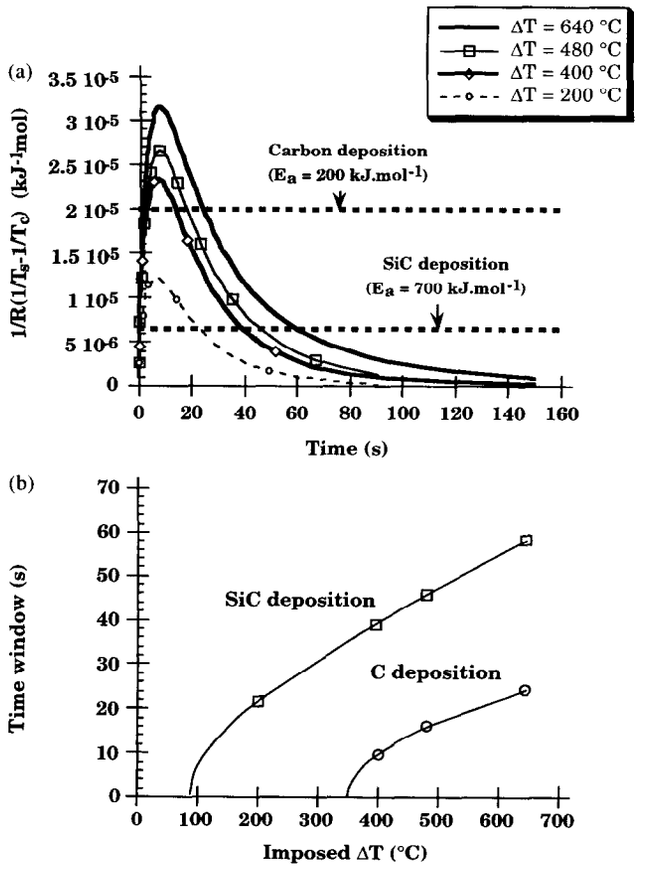

Fig. 9. Curves for a determination of an efficient pressure pulsing time window (a), and efficient pressure pulsing time windows as a function of the imposed temperature difference (b).

preform is 100 times longer. Such a situation has advantages and drawbacks. First, the time needed to heat the preform *in vacuo* is much longer, which is an adverse effect. But then, the persistence of a gradient inside the preform should also be increased, and this is a positive effect. One could expect that many more pressure pulses could be applied to the preform during the cooling of the preform. Also, the maximal efficiency of the imposed temperature difference should be enhanced, with the consequence that the inversed-gradient CVI would be more easily feasible for low-E_a chemical deposition kinetics, as is the case for pyrocarbon.

4 Experimental Infiltration

Silicon carbide and carbon matrix composites are used in a variety of applications including rocket motor nozzles, spacecraft thermal protections, brake disks, etc.[16–18] In such a scope, two series of experimental infiltration were studied: pyrocarbon and silicon carbide materials were deposited by a TP–CVI technique in carbon preforms.

4.1 Experimental and characterization procedure

4.1.1 Experimental apparatus

A schema of the apparatus, used for the TP–CVI process, is shown in Fig. 10(a). The reactor is a silica glass tube (internal diameter: 25 mm) heated externally. The deposition chamber is isothermal ($\pm 5°C$) over a height of 50 mm, and it shows a temperature gradient out of this zone [Fig. 10(b)] which is utilized to allow thermal cycling of the preform. The temperature is monitored using a thermocouple.

Mass and ball flowmeters are used to control the flowrates of the various gaseous species: propane, MTS (methyltrichlorosilane, CH_3SiCl_3) and hydrogen (carrier gas when using MTS). MTS is evaporated in a drying oven (it is liquid at room temperature and atmosphere pressure) and its vapor is then mixed with hydrogen in a heated and pressure regulated reservoir where it is stored before its admittance in the infiltration chamber, via an upper inlet pneumatic valve. The dilution α-ratio, defined as $\alpha = Q_{H_2}/Q_{MTS}$, where Q_{H_2} and Q_{MTS} are the gas flows of hydrogen and MTS, respectively, characterizes the composition of the gas phase used in the infiltration of SiC. The thermal gradient effect is achieved by periodically removing the preform from the hot zone (with the help of the piston device [Fig. 10(c)] to a cooler zone. Two compressed air inlet valves, ensure the rise and the descent of the piston.

Preforms used in this study are three-dimensional carbon fibres preforms*, described in Table 1. Their average mass is 2·82 g.

4.1.2 Characterization procedures

Each experiment is characterized by several parameters, namely:

- P, the deposition pressure, which must be low enough to make easier the gas phase infiltration;
- T, the deposition temperature;
- ΔT, the temperature quenching interval;
- α, the hydrogen/MTS ratio, which permits to modify the composition and microstructure of the SiC-based deposits;
- N, the total number of pressure pulses;
- N_p, which represents the number of pressure cycles during the quenching period. The increase of N_p allows to decrease the total infiltration time, while keeping the thermal quenching effect;
- t_g, t_a, t_r, t_p and t_e, the gradient establishment time, the admission time, the residence time, the evacuation time and the stability time, respectively.

After densification, the preforms were cut in order to study by Scanning Electron Microscopy† (SEM) the densification gradient. For these SEM observations, polished specimen cross-sections were prepared using standard metallographic techniques (embedding in a resin, then mechanically polishing from 75 to 5 μm grade diamond disks and pastes). Then, the specimens were coated with a thin layer of Au-Pd or C to facilitate observations.

The pyrocarbon (PyC) microstructure, resulting from the cracking of propane, was studied by the measurement, with an optical microscope,‡ of polished cross-sections of preforms, in polarized light, of the extinction angle, Ae, characteristic of the PyC anisotropy. A classification has been defined to characterize the different PyC textures:[19]

- Rough laminar (RL) $18° \leq Ae \leq 25°$
- Smooth laminar (SL) $13° \leq Ae < 18°$
- Dark laminar (DL) $4° \leq Ae \leq 12°$
- Isotropic (I) $Ae < 4°$

The SiC microstructure was also studied. It has been assessed by X-ray diffraction§ (XRD method: Cu K_α, $\lambda = 1{\cdot}54$ Å).

*From S.E.P.
†JEOL 840 and Hitachi s-4500.
‡MeF3 from Reichert-Jung.
§D 5000 from Siemens.

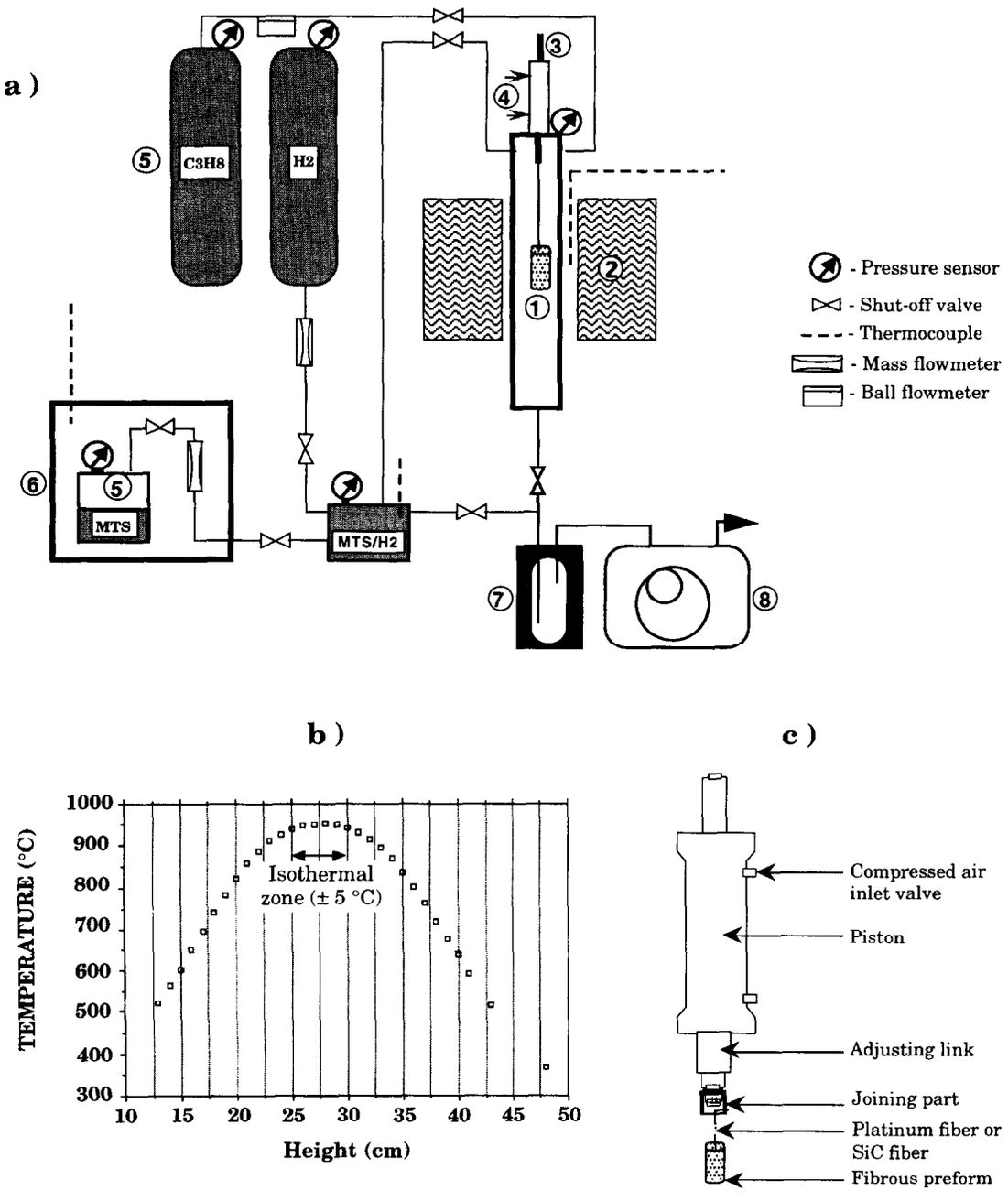

Fig. 10. The P–CVI apparatus used for the densification of the carbon fibrous preform: (a) schematic, (b) temperature axial profile and (c) piston device to move the preform. (1: fibrous preform; 2: furnace; 3: piston; 4: compressed air inlet valves; 5: sources gas; 6: drying oven; 7: liquid nitrogen trap; 8: rotary vacuum pump.)

For each densified preform, several parameters were calculated in order to compare the different experiments:

- the *relative mass uptake*, $\Delta m/m_i$, after infiltration:

$$\Delta m/m_i\% = (m_f - m_i)/m_i \tag{8}$$

where m_i and m_f are the initial and the final preform mass, respectively.

- the *normalized mass uptake*, μ, is defined as a $\Delta m/m_i$ for 2000 pulses:

$$\mu = (\Delta m/m_i).\frac{2000}{N} \tag{9}$$

where N is the total number of pulses.

- the evaluation, by SEM, of the *deposit thicknesses* on the fibres, in the core, the middle and at the surface of the densified preforms.
- the *pulse efficiency*, R_p, which represents the effective deposition time in comparison with the complete time of each cycle:

$$R_p = t_r/\sum_i t_i \tag{10}$$

- and the *total time*, t_w, of the P–CVI cycles, during thermal quenching:

$$t_w = \sum_i (t_{ai} + t_{ri} + t_{pi}) \quad (11)$$

Moreover, in order to compare the TP–CVI technique with other processes, a few experiments were achieved without temperature quenching interval (i.e. by P–CVI).

Lastly, in order to provide a quantitative evaluation of the thickness gradient, a reduced variable has been defined by systematically dividing the thicknesses by the thickness at the surface. This variable, denoted as center-to-surface thickness ratio, has been calculated for the TP–CVI experiments.

4.2 Experimental results and discussion

4.2.1 Preliminary experiments by P–CVI

Five experiments were first carried out according to a P–CVI route. The experimental conditions and results of these PyC and SiC P–CVI deposition are listed in Table 2. The experimental conditions for SiC deposition were established by Lespiaux,[20] Loumagne[21] and Heurtevent *et al.*[22] In the same way, the experimental conditions for PyC deposition have been deduced from Dupel *et al.* works.[12,13,19]

The results for PyC deposits show that very good mass uptake was obtained with short densification times ($\leq$ 5 h). Nevertheless, the deposit thicknesses were relatively low (of the order of one micrometer) and the PyC deposit preferentially localized at the preform periphery. Furthermore, the normalized mass uptake (μ) is very variable. An increase of the deposition pressure (runs #3 and #4) contributes to decrease the normalized mass uptake (by $\approx$16%). An increase of the deposition temperature (runs #2 and #4) contributes to increase the normalized mass uptake and the homogeneity of the deposit.

Concerning the SiC deposition experiments (run #5 in Table 2), the same conclusions can be drawn, that is to say, a thickness negative gradient from the core to the preform surface, referred to as a normal gradient in as much as it is what usually happens in conventional CVI-processes [Fig. 11a]. The graph in Fig. 11(b) shows the relative deposit thickness (in the core, middle and surface) in the densified preform.

During densification by P–CVI, the preform is maintained at an uniform temperature, and this for each pulse. Under such conditions, diffusive transport leads to a quicker densification at the preform periphery. Only convective transport would enhance densification in the core of the preform, but it appears not to be sufficient to invert the densification gradient in our experimental conditions. This is consistent with former theoretical predictions[23] and experimental studies.[12,13]

4.2.2 Determination of the TP–CVI optimal infiltration conditions

The experimental conditions used for the preliminary experiments to deposit SiC and PyC materials by a pulsed-CVI technique were determined by seeking an optimum in the infiltration quality. However, the transposition of these P–CVI conditions to TP–CVI is not straightforward. Indeed, crudely applying P–CVI conditions to pyrocarbon TP–CVI led to the formation of tars and soot; so, operating temperature and pressure had to be modified. The characteristic times of the TP–CVI pulse (t_a, t_g, t_r, t_p and t_e, see section 4.1.2 and Table 3) were also associated to these physicochemical conditions. A reference pulse number of about 2000 was chosen. It can be noted that the rise or the descent of the piston is accomplished in 1·5 s each.

An adequate set of operating conditions for the TP–CVI experiments is shown in Table 3. The gradient creation time (t_g) has been fixed at 0·5 s: this time taking into account the response time of the pneumatic valve which monitors the rise of the piston. The admission time (t_a) was also fixed at 0·3 s, for each experiment. The evacuation time (t_p), which varies from 2 to 10 s, depends on the pumping capacity of the rotary pump. The reduction of this evacuation time is necessary to improve

Table 2. Experimental conditions[a] and results for the PyC and SiC P–CVI deposition

Series	*Deposit*	P *(kPa)*	T *(°C)*	N	α[b]	R*p* *(%)*	$\Delta m/mi$ *(%)*	μ *(%)*	*Relative deposit thickness*			*Surface thickness* (μm)
									Core	*Middle*	*Surface*	
1	PyC	3	930	2000		31·7	8	8	0·25	0·50	1	0·4
2	PyC	11	980	2250		27·4	69	61	0·47	0·52	1	1·25
3	PyC	8	1030	1800		27·4	98	109	0·83	0·86	1	1·25
4	PyC	11	1030	2250		27·4	103	92	0·57	0·64	1	1·4
5	SiC	10	1030	2000	6	27·4	60	60	0·29	0·36	1	1·4

[a] t_a = 0·3 s; t_p = 5 s; t_r = 2 s, except for series N°1 where t_r = 1 s.
[b] In the initial gas phase.

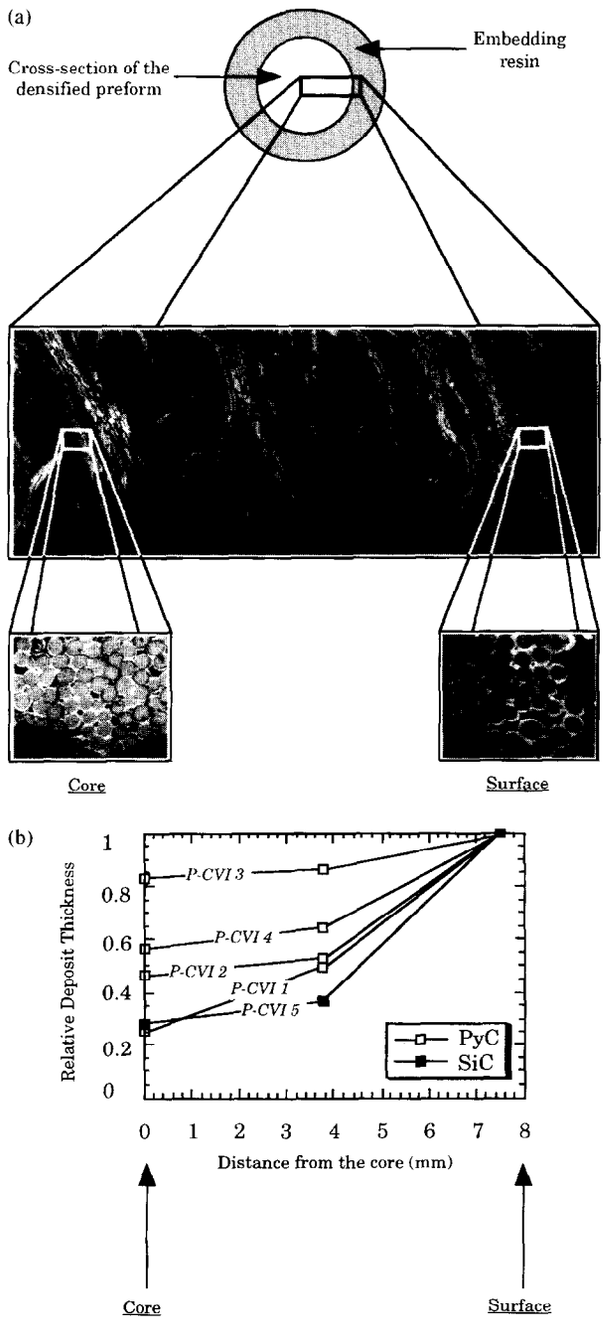

Fig. 11. SEM observation of a preform cross-section densified with a P–CVI route, and thick gradient: (a) SEM images of the densified preform (PyC deposit) and (b) deposit thickness gradient across the preform.

the efficiency (R_p) of the TP–CVI technique, because this step is not a deposition phase. The temperature quenching interval, ΔT, was chosen from 50°C to 400°C, in accordance with the effective thermal gradient evaluation. A stability time, t_e, from 15 s to 40 s was necessary to allow the preform core to reach a high and uniform temperature.

4.2.3 Discussion of the TP–CVI results

The experimental conditions and results for each experimental infiltration, are collected in Table 4, and plotted in Fig. 12.

Table 3. Parameters for PyC and SiC TP–CVI deposition

	Deposition parameters	*Deposit type*	
		SiC	*PyC*
T	Deposition temperature (°C)	1030–1100	1030–1100
ΔT	Temperature quenching interval (°C)	50–400	100–400
P	Deposition pressure (kPa)	10–16	10–20
	Precursor gas	$MTS+H_2$	C_3H_8
α	Hydrogen/MTS ratio	1–6	
N	Pulse number	1980–2075	1115–5800
Np	Pulse-mode	2–5	1–5
t_g	Gradient creation duration (s)	0·5	0·5
t_a	Admission time (s)	0·3	0·3
t_r	Residence time (s)	1·5	1·5–2
t_p	Evacuation time (s)	3–5	2–10
t_e	Stability time (s)	15–20	15–40

4.2.3.1 Influence of ΔT *on the deposition gradient.* First, the main parameter, i.e. the temperature quenching interval ΔT, determines the nature of the densification gradient.

It appears from Fig. 12(a) that the value of ΔT inverting the densification gradient is approximately 300°C for pyrocarbon whereas it should be superior to 100°C for the SiC. Also, the effect of ΔT on the densification gradient is much stronger for SiC than for PyC, as expected from the activation energies. These experimental results confirm the thermal evaluations: indeed, Fig. 8 has shown that the TP–CVI of PyC was only feasible when $\Delta T > 350$°C; whereas in the case of the TP–CVI of SiC, a more moderate value of ΔT ($\Delta T > 100$°C) was adequate. But, for the TP–CVI of SiC, the inversion of the thickness gradient depends on other experimental conditions such, as the H_2/MTS ratio, α, which also modifies strongly the thickness gradient.

Figure 13 shows the cross-sections of an infiltrated preform after 1980 TP–CVI SiC infiltration pulses (run #18). In these photographs, a strong densification gradient is observed. Indeed, it seems that only the center of the preform has been densified.

An important feature of TP–CVI appears by comparing experiments 6 and 7, which only differ by the duration (2020 pulses for #6 and 5800 for #7): at a more advanced densification stage, the (inverted) gradient is lesser. This is easy to understand on the basis that a rapidly densified core becomes less penetrable and evolves in a slower fashion at further densification stages.

As far as we were primarily interested in obtaining inverse thickness gradients, we did not perform a thorough study of the influence of less important parameters. However, some tendencies may be drawn from our experiments.

Table 4. Experimental conditions and results for PyC and SiC TP–CVI deposition

Series	Deposit	T (°C)	ΔT (°C)	P (kPa)	t_r (s)	t_p (s)	t_e (s)	t_w (s)	N	N_p	α	R_p (%)	Δm/mi (%)	μ (%)	Thickness gradient	Relative deposit thickness			Surface thickness (μm)
																Core	Middle	Surface	
1	PyC	1030	100	10	2	3	20	26·5	2035	5		20	39	38·3	Normal	0·50	0·60	1	1·1
2	PyC	1030	200	10	2	3	20	26·5	1310	5		20	9	13·7	Normal	0·67	0·80	1	0·88
3	PyC	1030	400	10	2	3	20	26·5	1100	5		20	2·5	4·5	Inverse	1·20	1·10	1	0·75
4	PyC	1030	400	11	2	10	40	12·3	2000	1		3·6	50	50	Inverse	1·49	1·27	1	1
5	PyC	1030	400	20	2	5	20	7·3	2020	1		6·5	25	24·8	Inverse	1·30	1·25	1	0·4
6	PyC	1030	400	20	2	5	40	7·3	2020	1		4	65	64·4	Inverse	1·35	1·14	1	1·6
7	PyC	1030	400	20	2	5	40	7·3	5800	1		4	144	49·7	Inverse	1·16	1·07	1	4·75
8	PyC	1065	400	10	1·5	2	15	7·6	2000	2		11·5	33	33	Inverse	1·35	1·20	1	0·2
9	PyC	1065	400	20	1·5	2	15	7·6	1628	2		11·5	34	41·8	Inverse	1·29	1·19	1	0·3
10	PyC	1100	400	10	2	3	20	26·5	1115	5		20	2·5	4·5	Inverse	1·30	1·20	1	0·4
11	PyC	1100	400	20	2	5	15	7·3	1675	1		7·8	66·7	79·6	Inverse	1·27	1·20	1	1·05
12	SiC	1030	50	10	1·5	3	20	24	2000	5	6	15·8	17	17	Normal	0·58	0·89	1	0·65
13	SiC	1030	100	10	1·5	3	20	24	2000	5	6	15·8	8	8	No gradient	1	1	1	0·35
14	SiC	1030	200	10	1·5	5	20	34	2000	5	1	13	93	93	Normal	0·34	0·67	1	1·2
15	SiC	1030	200	10	1·5	5	20	34	2000	5	2	13	43·2	43·2	Inverse	5·8	4	1	0·1
16	SiC	1030	200	10	1·5	5	20	34	2000	5	6	13	2·1	2·1	Inverse	4	3	1	0·1
17	SiC	1030	200	16	1·5	5	20	34	2000	5	1	13	90	90	Normal	0·2	0·34	1	2·14
18	SiC	1030	400	10	1·5	3	15	9·6	1980	2	6	10·7	1·6	1·6	Inverse	3·25	1·2	1	0·6
19	SiC	1030	400	10	1·5	3	20	24	2000	5	6	15·8	2	2	Inverse	2·5	1·5	1	0·08
20	SiC	1100	200	10	1·5	3	20	24	2075	5	6	15·8	3	2·9	Inverse	3·9	1	1	0·1

4.2.3.2 Temperature. From runs #3 and #10, for the TP–CVI of PyC, and from runs #16 and #20, for the TP–CVI of SiC, it appears that the normalized mass gain is almost the same at 1030°C and 1100°C. The center-to-surface thickness ratios are likewise quasi-identical. So, the deposition temperature seems to be a less limiting experimental parameter, at least in the rather narrow range of our study.

4.2.3.3 Pressure. The pressure has been varied from 10 to 20 kPa for PyC TP–CVI deposition (runs #8 and #9 for $T = 1065$°C and runs #4 and #6 for $T = 1030$°C) and from 10 to 16 kPa for SiC TP–CVI deposition (runs #14 and #17).

For the TP–CVI of PyC, the deposition pressure increase results in an increase of the normalized mass uptake (of about 30%), and a decrease of the thickness gradient, i.e. the center-to-surface

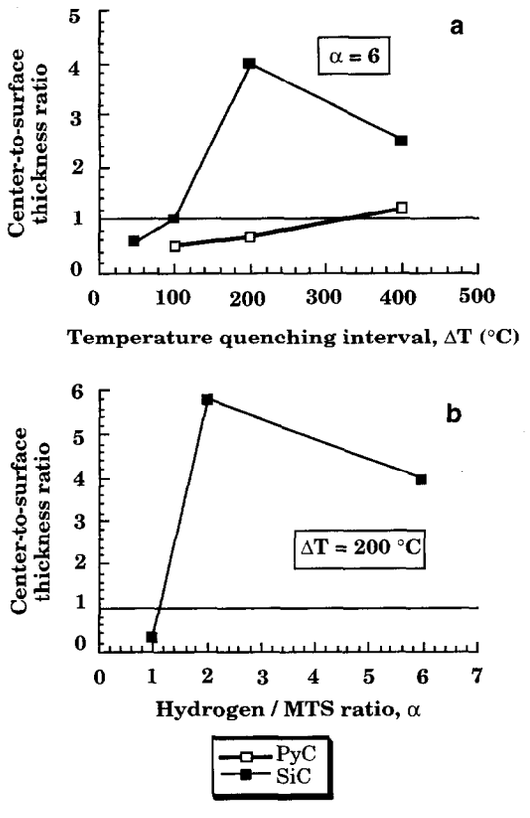

Fig. 12. Evolution of the center-to-surface thickness ratio with (a) the imposed temperature quenching interval (ΔT) and (b) the SiC-dilution ratio (α).

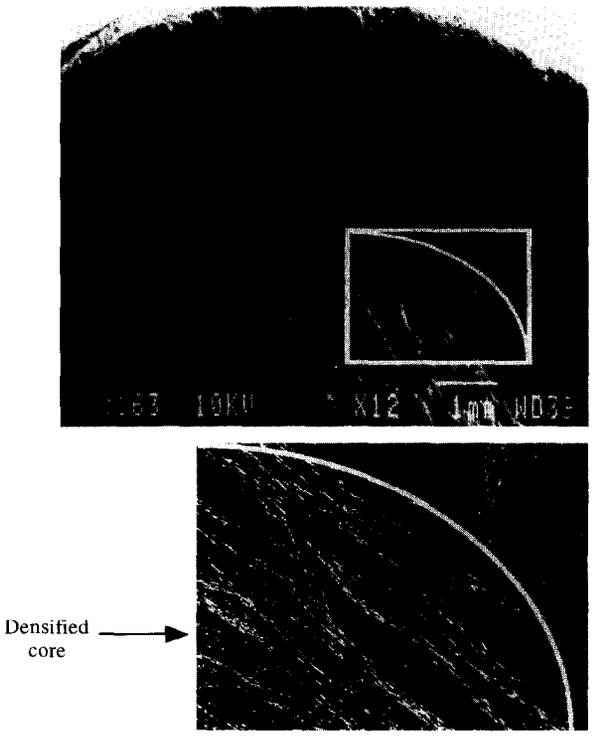

Fig. 13. SEM images showing the inversed thickness gradient during a SiC TP–CVI experiment (Series N°18, in Table 4).

thickness ratio is higher for $P = 10\,kPa$ than $P = 20\,kPa$.

For the TP–CVI of SiC, the center-to-surface thickness ratio does not seem to depend on the total pressure (at least in conditions leading to a normal gradient).

The influence of the propane partial pressure on the PyC thickness profile along straight pores with rectangular cross-sections has been experimentally and theoretically studied by Dupel *et al.*[13] The PyC thickness profiles, along a $60\,\mu m$ model pore, has been studied, as a function of the temperature ($T = 950°C$ and $T = 1050°C$) and the pressure ($P = 1$, 3, 10, 50 and 100 kPa), for a residence time of 10 s. The main result was that decreasing the pressure in the infiltration chamber strongly reduced the thickness gradient along the pore, and so significantly improved the quality of the pore infiltration. For an inverted gradient, we obtain opposite results: for a higher deposition pressure, the center-to-surface thickness ratio is less pronounced. In all cases, the results may be understood on the basis of a less favoured diffusive transport when pressure increases.

4.2.3.4 Dilution ratio for SiC deposits. From runs #14, #15 and #16, it can be observed that the normalized mass gain increases strongly when the concentration of MTS increases (i.e. when α decreases), as shown in Fig. 12(b). When the dilution ratio decreases, the MTS concentration increases; so, the gas phase, enriched in SiC-gas precursor, contributes to form a thicker SiC deposit. Nevertheless, when $\alpha = 1$, the high concentration of MTS in the gas phase does not permit to invert the thickness gradient, in spite of a sufficient ΔT value. There seems to exist an optimum ratio, for which the center-to-surface thickness ratio is maximal (for $\alpha \approx 2$).

4.2.3.5 Experiment times (t_g, t_a, t_r, t_p, t_e and t_w). The influence of the various experiment times is less pronounced. Our main concern is only to reduce the deposit times which do not contribute to the densification (t_g, t_p) in order to increase the efficiency R_p. However, the stability time t_e, could not be decreased because it governs the efficiency of the densification for the next cycle of pulses.

The total time t_w, reported in Table 4, can be compared to the time window, defined in Section 3.5. It is not easy to relate the influence of the total time t_w, to the normalized mass uptake and the final filling. For the SiC experiments, the effect of the total time tw and the dilution ratio cannot be distinguished. In both cases, it seems that the evaluations of t_w presented in Fig. 9 are too small. As an example, for PyC growth at $\Delta T = 400°C$, the predicted t_w was 10 s, and inverted gradient densifications were observed with $t_w = 26{\cdot}5$ s.

Table 5. Values of the extinction angle Ae for the PyC P–CVI and TP–CVI deposition

Experiments	*Series*	*Ae (°)*
P–CVI	2	13
P–CVI	3	15
P–CVI	4	15
TP–CVI	4	12
TP–CVI	6	13
TP–CVI	7	15
TP–CVI	10	15

4.2.4 Morphology of deposits

A structural analysis of the PyC deposited during the P–CVI and TP–CVI experiments was carried out in order to evaluate the deposit quality. The values of the extinction angle Ae are given in Table 5. The PyC microstructures deposited either by P–CVI or TP–CVI are all the same, i.e. a smooth laminar texture-type. For SiC deposition, the β-SiC crystallite mean size-L_{111}, was measured by X-ray diffraction (with the Scherrer equation). It is equal to 15–30 nm. These SiC deposits are in fact a co-deposit of SiC and C, i.e. a carbon-rich SiC deposit.

5 Conclusion

It has been demonstrated that a new CVI technique, in which a thermal gradient is associated with the repetitive introduction of the reactant gases, is capable of producing in fibre preforms deposits having an inverse density gradient. It has been clearly demonstrated both experimentally and theoretically that if the temperature quenching interval ΔT exceeds a critical value, depending primarily on the activation energies of the deposition kinetics, then the densification becomes quicker in the core of the preform. Other experimental parameters have been studied. For SiC deposition, the second most important parameter is the dilution α-ratio, while for PyC deposition, it is the total pressure.

Acknowledgement

The authors wish to thank M. Alrivie for help in the preparation of specimens.

References

1. Lackey, W. J., Review, status and future of the chemical vapor infiltration process for fabrication of fibre-reinforced ceramic composites. *Ceram. Eng. Sci. Proc.*, 1989, **10**(7–8), 577–584.
2. Roman, Y. G. and Terpstra, R. A., Chemical vapour infiltration. *Ceramic Process Technology International*, 1996, 113–116.

3. Naslain, R., Langlais, F. and Fedou, R., The CVI-processing of ceramic matrix composites. *Journal de Physique, Colloque C5, Supplément au n5*, 1989, **50**, 191–207.
4. Chang, H. C., Morse, T. F. and Sheldon, B. W., Minimizing infiltration times during the initial stage of isothermal chemical vapor infiltration. *J. Materials Proc. and Manuf. Sci.*, 1994, **2**, 437–454.
5. Besmann, T. M., Lowden, R. A., Stinton, D. P. and Starr, T. L., A method for rapid chemical vapor infiltration of ceramic composites. *Journal de Physique*, 1989, Colloque C5, Supplément au n°5, **50**, 229–239.
6. Besmann, T. M., McLaughlin, J. C. and Lin, H. T., Fabrication of ceramic composites: forced CVI. *Journal of Nuclear Materials*, 1995, **219**, 31–35.
7. Stinton, D. P., Lowden, R. A. and Besmann, T. M., Fibre-reinforced tubular composites by CVI. *Mat. Res. Soc. Symp. Proc.*, 1992, **250**, 233–238.
8. Bryant, W. A., Producing extended area deposits of uniform thickness by a new chemical vapor deposition technique. *Journal of Crystal Growth*, 1976, **35**, 257–261.
9. Sugiyama, K. and Yamamoto, E., Reinforcement and antioxiding of porous carbon by pulse CVI of SiC. *J. Mat. Sc.*, 1989, **24**(10), 3756–3762.
10. Sugiyama, K. and Yamamoto, E., Pulse CVI of SiC to porous carbon. In *Proceedings of the 10th International Conference on Chemical Vapor Deposition*, Honolulu, (October 1987), ed. G. W. Cullen in *The Electrochemical Society*, NJ, 1987, pp. 1041–1049.
11. Itoh, K., Imuta, M., Sakai, A., Gotoh, J. and Sugiyama, K., Pulsed chemical vapour infiltration of SiC to three-dimensional carbon fibre preforms. *J. Mat. Sci.*, 1992, **27**, 6022–6028.
12. Dupel, P., Pailler, R. and Langlais, F., Pulse chemical vapour deposition and infiltration of pyrocarbon in model pores with rectangular cross-sections—Part 1: Study of the pulsed process of deposition. *J. Mat. Sci.*, 1994, **29**(5), 1341–1347.
13. Dupel, P., Pailler, R., Bourrat, X. and Naslain, R., Pulse chemical vapour deposition and infiltration of pyrocarbon in model pores with rectangular cross-sections—Part 2: Study of the infiltration. *J. Mat. Sci.*, 1994, **29**(4), 1056–1066.
14. Tomadakis, M. M. and Sotirchos, S. V., Transport properties of random arrays of freely overlapping cylinders with various orientation distributions. *J. Chem. Phys.*, 1993, **98**(1), 616–626.
15. Josiek, A. and Langlais, F., Residence-time dependent kinetics of CVD growth of SiC in the MTS/H_2 system. *J. Crystal Growth*, 1996, **160**, 253–260.
16. Choury, J. J., SEP carbon and ceramic composites in aeronautics and space applications. In *Proc. 1st. Int. Symp. Functionally Gradient Materials*, ed. M. Yamanouchi, M. Koizumi, T. Hirai and I. Shiota, in *Soc Non Tradit. Technology*, Tokyo, 1990, p. 157.
17. Upadhya, K., Ceramics and composites for rocket engines and space structures. *J. of Mat.*, 1992, **44**(5), 15–18.
18. Fuentes, R. I., Silicon carbide: advanced material—applications and preparation. *Chemistry and Industry*, 1992, **21**, 806–808.
19. Dupel, P., Bourrat, X. and Pailler, R., Structure of pyrocarbon infiltrated by pulse-CVI. *Carbon*, 1995, **33**(9), 1193–1204.
20. Lespiaux, D., Processus de nucléation/croissance et caractérisation microstructurale de céramiques base SiC obtenues par CVD/CVI dans le système Si-C-H-Cl. Ph.D. Thesis, University of Bordeaux I, 1992.
21. Loumagne, F., CVD du carbure de silicium à partir de CH_3SiCl_3/H_2: Processus homogènes et hétérogènes—caractérisation microstructurale. Ph.D. Thesis, University of Bordeaux I, 1993.
22. Heurtevent, F., Matériaux multicouches nanoséquencées $(PyC/SiC)_n$.—application en tant qu'interphases dans des composites thermostructuraux. Ph.D. Thesis, University of Bordeaux I, 1996.
23. Sotirchos, S. V., Chemical Vapor Infiltration under pressure pulsing conditions. In *High Temperature Ceramic Matrix Composites*, ed. R. Naslain, J. Lamon and D. Doumeingts. Woodhead Publishing Ltd., 1993, pp. 241–248.